International Symposium
On Turbulence and Shear Flow
Phenomena (TSFP-8)
August 28 - 30, 2013 Poitiers, France

STIRRING AND MIXING BY GRID-GENERATED TURBULENCE IN THE PRESENCE OF A MEAN SCALAR GRADIENT

Sylvain Laizet
Turbulence, Mixing and Flow Control Group,
Department of Aeronautics, Imperial College London
London, SW7 2AZ, United Kingdom
s.laizet@imperial.ac.uk

J.Christos Vassilicos
Turbulence, Mixing and Flow Control Group,
Department of Aeronautics, Imperial College London
London, SW7 2AZ, United Kingdom
j.c.vassilicos@imperial.ac.uk

ABSTRACT

The stirring and mixing of a passive scalar by grid-generated turbulence in the presence of a mean scalar gradient is studied in three dimensions by DNS (Direct Numerical Simulation). Using top-end high fidelity computer simulations, we calculate and compare the effects of various fractal and regular grids on scalar transfer and turbulent diffusion efficiencies. We demonstrate the existence of a new mechanism present in turbulent flows generated by multiscale/fractal objects which has its origin in the multiscale/fractal space-scale structure of such turbulent flow generators. As a result of this space-scale unfolding (SSU) mechanism, fractal grids can enhance scalar transfer and turbulent diffusion by one order of magnitude while at the same time reduce pressure drop by half. The presence of this SSU mechanism when turbulence is generated by fractal grids means that the spatial distribution of length-scales unfolds onto the streamwise extent of the flow and gives rise to a variety of wake-meeting distances downstream. This SSU mechanism must be playing a decisive role in environmental, atmospheric, ocean and river transport processes wherever turbulence originates from multiscale/fractal objects such as trees, forests, mountains, rocky river beds and coral reefs. It also ushers in the new concept of fractal design of turbulence which may hold the power of setting entirely new mixing and cooling industrial standards.

INTRODUCTION

Recently, Hurst & Vassilicos (2007); Mazellier & Vassilicos (2010); Nagata *et al.* (2008); Nicolleau *et al.* (2011); Valente & Vassilicos (2011); Gomes-Fernandes *et al.* (2012) used different multiscale grids to generate turbulence in a wind tunnel or in a water tank and have shown that complex multiscale boundary/initial conditions can drastically influence the behaviour of a turbulent flow, especially when a fractal square grid (see figure 1) is placed at the entry of a wind tunnel test section. Fractal geometry is a concept where a given pattern is repeated and split into parts, each being a reduced-copy of the whole. Multiscale (fractal) objects can be designed to be immersed in any fluid flow where there is a need to control and design the turbulence generated by the object. The experiments have shown that, unlike regular objects (where the turbulence is generated by only one scale), a slight modification of one of the multiscale object's parameters can deeply modify the turbulence generated by the fluid's impact on the object. Multiscale objects offer the opportunity to discover new complex flow effects/interactions that can help understand how to control and/or manage complex fluid flows. Furthermore, such multiscale objects can be designed as energy-efficient mixers with high turbulent intensities and a small pressure drop, see Laizet & Vassilicos (2012). Coffey *et al.* (2007) have also shown experimentally that fractal grids can be designed as stirring elements for inline static mixers and, as such, that they compare favourably with commercially available state-of-the-art stirring elements.

In this computational study we calculate and compare the effects of various fractal and regular grids on scalar transfer and turbulent diffusion efficiencies (Shraiman & Siggia (2000); Warhaft (2000); Suzuki *et al.* (2010)). As a result we report on a new mechanism which greatly increases scalar transfer and turbulent diffusion and at the same time reduces pressure drop and therefore power losses.

The organisation of this paper is as follows. In the following section, we present the DNS methodology, a brief description of the grids and the numerical parameters of each simulation. Some results about the turbulence and the flow field downstream of the grid are discussed in the following section. Then, passive scalar results are presented, followed by a conclusion.

FLOW PARAMETERS AND NUMERICAL MODELLING

Numerical Methods

To solve the incompressible Navier-Stokes equations and the transport equation for the passive scalar, we use a numerical code (called **Incompact3d**) based on sixth-order

	$n_x \times n_y \times n_z$	$L_x \times L_y \times L_z$ (t_{min})	Grid	It.	κ	S t_{min}	σ	M_{eff}
DNS1	2305×288×288	768×96×96	□	3	10ν	1/16	0.3	$14.7t_{min}$
DNS2	2305×288×288	768×96×96	I	3	10ν	1/16	0.3	$23.4t_{min}$
DNS3	2881×360×360	1152×144×144	□	4	10ν	1/16	0.5	$6.5t_{min}$
DNS4	2881×180×180	1152×72×72	Reg.		10ν	1/16	0.5	$6.5t_{min}$

Table 1. Numerical parameters of the simulations and characteristics of the grids.

compact schemes for spatial discretization and a third order Adams-Bashforth scheme for time advancement. To treat the incompressibility condition, a fractional step method requires to solve a Poisson equation. This equation is fully solved in spectral space, via the use of relevant 3D Fast Fourier Transforms. The pressure mesh is staggered from the velocity mesh by half a mesh, to avoid spurious pressure oscillations. With the help of the concept of modified wave number, the divergence free condition is ensured up to machine accuracy. More details about the present code and its validations, especially the original treatment of the pressure in the spectral space, can be found in Laizet & Lamballais (2009). The modelling of the grids is performed by an Immersed Boundary Method, following a procedure proposed by Parnaudeau *et al.* (2008). The present method is a direct forcing approach that ensures the no-slip boundary condition at the grid walls. It mimics the effects of a solid surface on the fluid with an extra forcing in the Navier-Stokes equations.

Because of the size of the simulations, the parallel version of **Incompact3d** has been used for this numerical work. Based on a highly scalable 2D decomposition library and a distributed FFT interface, it is possible to use the code on thousands of computational cores. More details about this efficient parallel strategy can be found in Laizet & Li (2011).

Governing equations

The governing equations for the incompressible velocity field are the forced Navier-Stokes equations:

$$\frac{\partial \mathbf{u}}{\partial t} = -\nabla p - \frac{1}{2}\left[\nabla(\mathbf{u}\otimes\mathbf{u}) + (\mathbf{u}.\nabla)\mathbf{u}\right] + \nu\nabla^2\mathbf{u} + \mathbf{f} \quad (1)$$

$$\nabla.\mathbf{u} = 0 \quad (2)$$

where $p(\mathbf{x},t)$ is the pressure field (for a fluid with a constant density $\rho = 1$) and $\mathbf{u}$ the velocity field. The forcing field $\mathbf{f}(\mathbf{x},t)$ is used through an Immersed Boundary Method in order to take into account the grid inside the computational domain. $\mathbf{x} \equiv (x,y,z)$ are the spatial coordinates in the streamwise (x) and two spanwise directions.

The scalar field $\theta(\mathbf{x},t)$ is advected by the velocity field and diffused by molecular processes, i.e. our code solves

$$\frac{\partial \theta}{\partial t} + \mathbf{u}\cdot\nabla\theta = \kappa\nabla^2\theta \quad (3)$$

with molecular diffusivity $\kappa = 10\nu$. The initial condition we impose on this scalar field is $\theta(\mathbf{x},0) = Sy$ where S is a constant scalar gradient and the inflow condition is $\theta = Sy$ at all time. The other boundary conditions for θ are outflow in the streamwise end of the computational domain, periodic in the z direction and an anti-symmetric conditions in the y direction. These conditions are the simplest way to initiate and sustain a turbulent scalar flux, see Corrsin (1952); Wiskind (1962); Warhaft (2000)

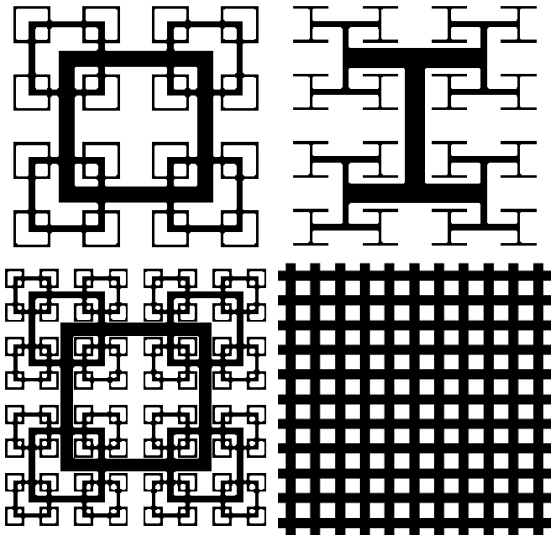

Figure 1. Scaled diagrams of the four grids used in this study. From left to right: fractal square grid with 3 fractal iterations, I grid with 3 fractal iterations, square grid with 4 fractal iterations and regular grid.

Numerical Parameters

As shown in Figure 1, four different grids are used in this numerical work to investigate the streamwise evolution of the stirring and mixing of a passive scalar in the presence of a mean scalar gradient. We considered two families of fractal grids each based on a different fractal-generating pattern, see Hurst & Vassilicos (2007). The two patterns can be distinguished by the number of rectangular bars they require, 3 for the I grid and 4 for the square grids. These fractal grids are completely characterised by the choice of the pattern and:

(i) the number of fractal iterations N, here $N = 3$ for the fractal I grid and $N = 3,4$ for the fractal square grids,
(ii) the bars' lengths $L_j = R_L^j L_0$ and lateral thicknesses $t_j = R_t^j t_0$ (in the plane of the grid, normal to the mean flow) at iteration j, $j = 0,\ldots,N-1$. Here, $R_L = 1/2$, $L_0 = 0.5L_y$ for all the fractal grids, where L_y and L_z (with $L_y = L_z$) are the lateral sizes of the computational domain. By definition, $L_0 = L_{max}$, $L_{N-1} = L_{min}$,

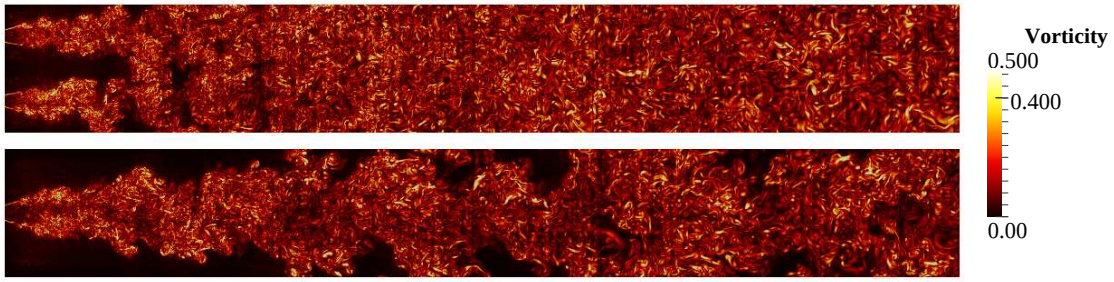

Figure 2. Instantaneous absolute value of the vorticity vector normalised by its maximum over the $(y-z)$ planes. Plots in the $(x-y)$ plane for $z = L_z/2$. Top: DNS1 with the fractal square grid with three fractal iterations and bottom: DNS2 with the I grid.

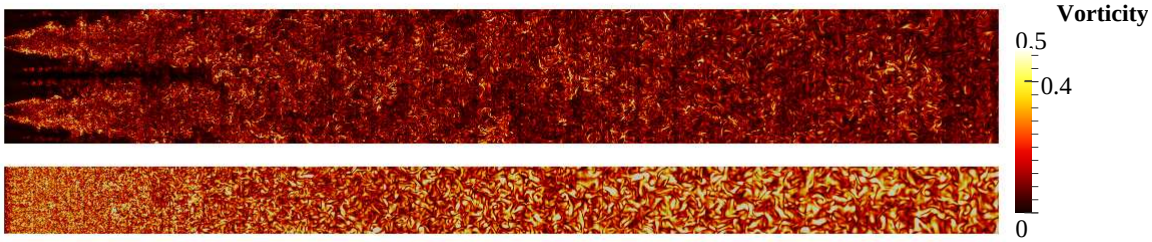

Figure 3. Instantaneous absolute value of the vorticity vector normalised by its maximum over the $(y-z)$ planes. Plots in the $(x-y)$ plane for $z = L_z/2$. Top: DNS3 with the fractal square grid with four fractal iterations and bottom: DNS4 with a regular grid.

$t_0 = t_{max}$ and $t_{N-1} = t_{min}$. Note that, in the present work, t_{min} is set to the same value for all fractal grids,
(iii) the number 4^j of patterns at iteration j
(iv) the thickness ratio $t_r \equiv t_{max}/t_{min}$, i.e. the ratio between the lateral thickness of the bars making the largest pattern and the lateral thickness of the smallest. $t_r = 8.67$ for the fractal square grid with three iterations, $t_r = 10.5$ for the fractal I grid and $t_r = 8.5$ for the fractal square grid with four fractal iterations.

The blockage ratio σ of our fractal grids defined as the ratio of their total area in the lateral plane to the area $T^2 = L_y \times L_z$, are determined by our choices of the previous parameters and are given in Table 1.

Unlike regular grids, multiscale/fractal grids do not have a well-defined mesh size. This is why Hurst & Vassilicos (2007) introduced an effective mesh size for multiscale grids, $M_{eff} = \frac{4T^2}{L_G}\sqrt{1-\sigma}$ where L_G is the perimeter length in the $(y-z)$ plane of the fractal grid. The multiscale nature of multiscale/fractal grids influences M_{eff} via the perimeter L_G which can be extremely long in spite of being constrained to fit within the area $T^2 = L_y \times L_z$. However, this definition of M_{eff} also returns the regular mesh size M, when applied to our regular grid. The effective mesh size is fully determined by our choices of parameters characterising the fractal grids and is given in Table 1. The regular grid considered here has the same blockage ratio as the fractal square grid with four iterations. The lateral thickness b of this regular grid is $2.6t_{min}$. Note finally that the streamwise thickness of the bars is $3.2t_{min}$ for all four grids used in this numerical study.

The computational domain and number of mesh nodes for each simulation are given in Table 1. For the velocity field, inflow/outflow boundary conditions are used in the x-direction and periodic boundary conditions in the y direction for $-L_y/2$ and $L_y/2$ and in the z direction $-L_z/2$ and $L_z/2$. For each grid, the simulation is performed with a Reynolds number $Re_{t_{min}} = 300$ (based on the smallest lateral thickness t_{min} of the fractal grids and the streamwise upstream velocity U_∞).

FLOW FIELD AND TURBULENCE

3D enstrophy visualisations of the turbulent flows generated by the regular grid and the three fractal square grids are shown in figures 2 and 3. In these figures we plot isosurfaces of the absolute value of the vorticity vector nor-

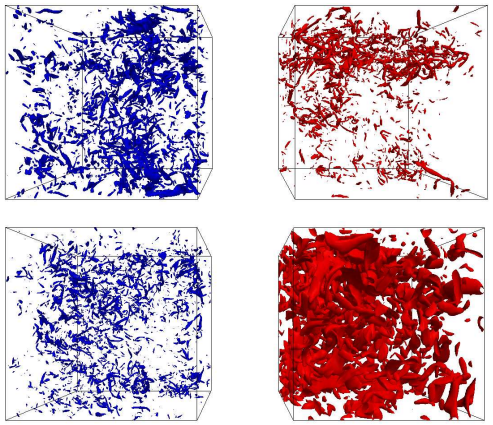

Figure 4. 3D isosurfaces for the absolute value of the vorticity vector normalised by its maximum over the $(y-z)$ plane in a 3D cube $L_y \times L_y \times L_z$ at the end of the computational domain. Top left: DNS1, top right: DNS2, bottom left: DNS3 and bottom right: DNS4. The isosurface is 0.5 in all four plots.

malised by its maximum over the y-z planes. These plots are in the $(x-y)$ plane for $z = L_z/2$. These isosurfaces are normalised in such a way that the decay of the turbulence is not visible on these plots. For the two grids with three fractal iteration (DNS1 and DNS2) and with the same blockage ratio, it can be seen that a non-homogeneous turbulent field is obtained close to the grids. In the case of the square grids (DNS2/DNS3), the turbulence does homogenise relatively close to the grid whereas for the I grid (DNS1) the influence of the grid and in particular of the biggest I can be seen until the end of the computational domain. For the regular grid, a conventional homogeneous istropic turbulence is obtained, with a streamwise increase of the size of the turbulent structures. Finally, it seems that the number of fractal iterations is playing a key role in the generation of the turbulence, as the two big wakes for DNS1 (three fractal iterations) and DNS3 (four fractal iterations) look quite different, with more pronounced streets of vortices for DNS1 in the first part of the computational domain.

The fact is also that these two different types of turbulent flows are generated in different ways. In the regular grid case, same-size wakes interact within a couple of mesh sizes from the grid and mix together in a uniform fashion close to the grid. In the fractal grid case, Laizet & Vassilicos (2009); Mazellier & Vassilicos (2010); Laizet & Vassilicos (2012) suggested that the smallest bars on the grid generate the smallest wakes which meet and mix together at the smallest distance from the grid, whereas larger bars generate larger wakes which meet and mix at a further distance from the grid, and that this process repeats itself from the smallest to the largest turbulence-generating scales on the grid in a way which causes the turbulence to progressively intensify over a protracted distance from the grid. We can therefore expect to have different behaviours for our passive scalar fields depending on the turbulent generator.

Figure 4 shows 3D isosurfaces of the absolute value of the vorticity vector normalised by its maximum over the $(y-z)$ plane in a 3D cube $L_y \times L_y \times L_z$ at the end of the computational domain. The one obvious difference in these visualisations between the turbulent flow generated by the regular grid and the turbulent flows generated by the fractal grids is that the latter are clearly more intermittent, especially for the fractal I grid (DNS2) where most of the structures in this particular visualisation are located near the top of the domain. The finest structures are obtained for the fractal square grid with four fractal iterations (DNS3) and the largest structures are obtained for the regular grid (DNS4).

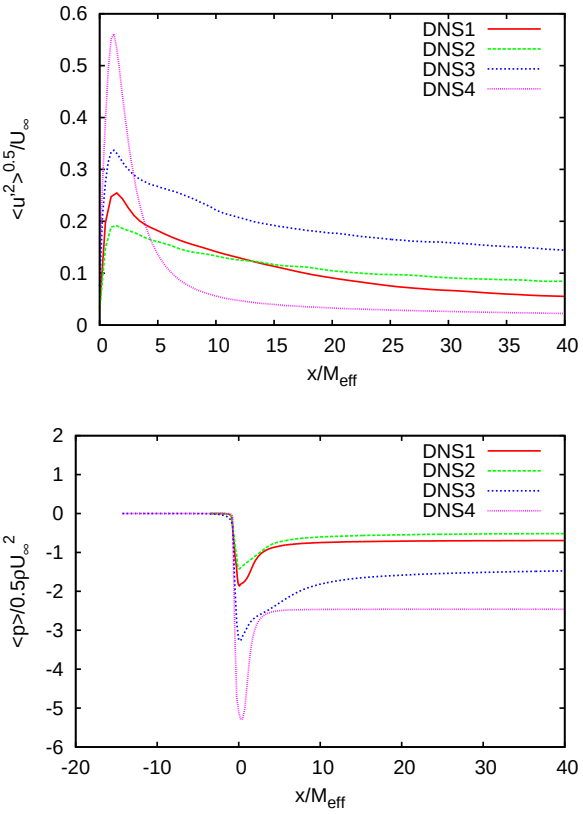

Figure 5. Streamwise evolution of $< u'^2 >^{0.5} /U_\infty$ (top) and $< p > /0.5\rho U_\infty^2$ (bottom) where $< . >$ denotes an average in y and z and over the collection time T.

Figure 5 shows the streamwise evolution of $< u'^2 >^{0.5} /U_\infty$ and $< p > /0.5\rho U_\infty^2$ (where p is the pressure divided by the fluid's mass density) for the four different grids with respect to x/M_{eff}. The regular grid generates a much higher peak average turbulence (more than 55%) than the three fractal grids. However, the average turbulence decay is much slower for the fractal grids whereas a very fast decrease can be observed for the regular grid. It should be noted that the spatial location of the peak of turbulence is approximately at a distance of $1M_{eff}$ from the grid for all four grids. At a distance of $35M_{eff}$ from the grid, the average turbulence for the fractal square grid with four fractal iterations is about 15% whereas for the regular grid it is only about 2.5% (same blockage ratio for the two grids). Another important result is the confirmation of the wind tunnel experiments of Hurst & Vassilicos (2007) that the I grid generates more turbulence on the centreline than the square grid, with a slower decay rate for the average turbulence.

The streamwise evolution of the pressure is consistent with the streamwise evolution of the average turbulence. For the regular grid the pressure drop is very important very close to the peak and then it remains constant at a low value whereas the three fractal square grids return a smaller pressure drop with a much longer pressure recovery length. As

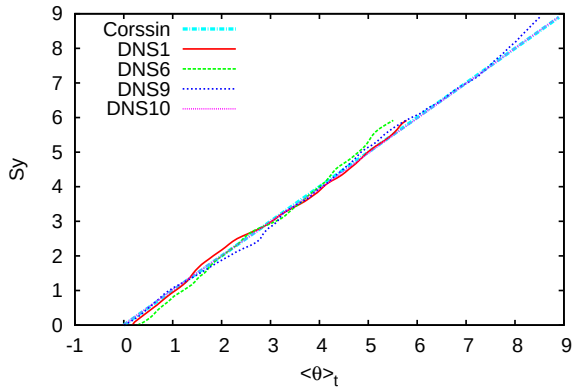

Figure 6. Profile in the y direction of $< \theta >_t + Sy$ at a streamwise location of $600t_{min}$ for $z = L_z/2$ where $< . >_t$ denotes an average in time only.

expected, DNS3 and DNS4 return a higher pressure drop than DNS1 and DNS2 (corresponding to the fractal grids with three fractal iterations) as their blockage ratio of 0.5 is higher than the one of 0.3 for DNS1 and DNS2. However, the pressure drop between upstream and far downstream in DNS3 is about half that for DNS4 even though the blockage ratio is the same. DNS1 and DNS2 have a similar low pressure drop even if the patterns of the grids are different.

PASSIVE SCALAR

The first important result concerning our passive scalar investigation is presented Figure 6. We find for our four grids that $< \theta >_t \approx Sy$. This first result is a non-trivial result reminiscent of one by Corrsin (1952) for homogeneous isotropic turbulence, see also Mydlarski & Warhaft (1998).

One interesting result about the passive scalar is presented in Figure 7 (top) where we can observe a continuous increase for the passive scalar variance, much more pronounced for the fractal grids. For instance, at the end of the computational domain, the variance is more than ten times bigger for the fractal grid with four fractal iterations (DNS3) than for the regular grid (DNS4). The monotonic increase of the passive scalar variance for the four grids is in qualitative agreement with the experiments of Sirivat & Warhaft (1983) where the variance was found to grow linearly with streamwise distance in decaying turbulent grid flow. Finally, it should be noted that the rate of increase is different for different grids.

The streamwise evolution of the normalised transverse turbulent scalar transfer $< v'\theta' > / \kappa S$ for the four different grids is plotted in Figure 7 (bottom). Different behaviours can again be observed: for the regular grid (DNS4), the normalised transverse turbulent scalar transfer peaks very close to the grid and then decay very quickly. For the fractal square grid with four fractal iterations (DNS3) and for the fractal I grid (DNS2), the normalised transverse turbulent scalar transfer peaks at a further distance from the grid, just before $200t_{min}$ and then remains approximately constant until the end of the computational domain. Finally, for the fractal square grid with three fractal iterations (DNS1), the normalised transverse turbulent scalar transfer also peaks just before $200t_{min}$ but then decay linearly from a value of about 15 to a value of about 7 at the end of the computational domain. The ratio of $< \theta'v' >$ for the fractal grid with four fractal iteration (DNS3) to $< \theta'v' >$ for the regular grid (DNS4) is oscillating between 19 at $x = 200t_{min}$ and 32 at the end of our computational domain.

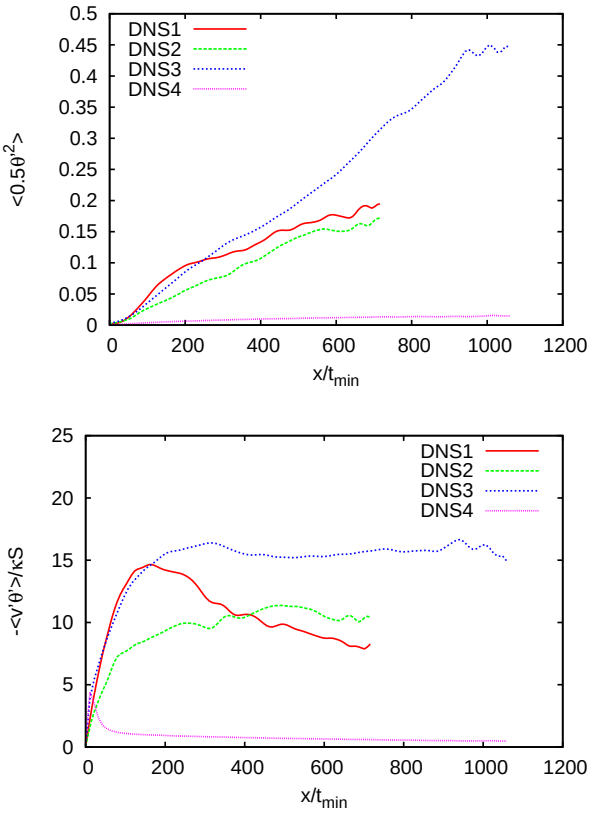

Figure 7. Streamwise evolution of the variance $\frac{1}{2} < \theta'^2 >$ (top) and of $< v'\theta' > \kappa S$ (bottom).

CONCLUSION

Four spatially evolving turbulent flows generated by three fractal grids and a regular grid have been investigated by means of Direct Numerical Simulation. We have focused on the stirring and mixing of a passive scalar in the presence of a mean scalar gradient. Different behaviours for different grids have been observed for the passive scalar variance and passive scalar flux.

The presence of the space-scale unfolding (SSU) mechanism introduced by Laizet & Vassilicos (2012) when turbulence is generated by fractal grids means that, for the same blockage ratio, the spatial distribution of length-scales on the fractal grid unfolds onto the streamwise extent of the flow and gives rise to a variety of wake-meeting distances downstream. As a result, the grid's turbulence generation is distributed in the streamwise direction causing the turbulence to be less and the pressure drop smaller very near the grid by comparison to a same blockage regular grid, but a much longer pressure recovery and a much slower turbulence decay in multiples of M_{eff}.

This mechanism is absent from regular grid turbulence where all wakes meet their neighboring wakes at the same short distance from the grid causing a great burst of intense turbulence very near the grid and a fast decay of this turbulence. The SSU mechanism is also responsible for the great scalar transfer enhancement caused by the fractal grids.

Further simulations will be required to investigate in more detail the SSU mechanism. In particular, it could be

interesting to change the boundary conditions for the passive scalar (wall in the y direction for instance) so that we can study the passive scalar variance decrease in the streamwise direction. Another future direction of investigation concerns the influence of the Prandtl number.

Acknowledgements

The authors are grateful to Dr. Ning Li for helping with the parallel version of **Incompact3d**. We also thank Eric Lamballais for very useful discussions and acknowledge support from EPSRC Research grants EP/E00847X/1 and EP/F051468/1.

REFERENCES

Coffey, C.J., Hunt, G.R., Seoud, R.E. & Vassilicos, J. C. 2007 Mixing effectiveness of fractal grids for inline static mixers. In *Proof of Concept report for the attention of Imperial Innovations.*. http://www3.imperial.ac.uk/tmfc/papers/poc.

Corrsin, S. 1952 Heat transfer in isotropic turbulence. *J. Applied Phys.* **33(1)**, 113–118.

Gomes-Fernandes, R., Ganapathisubramani, B. & Vassilicos, J. C. 2012 PIV study of fractal-generated turbulence. *J. Fluid Mech.* **701**, 306–336.

Hurst, D. & Vassilicos, J. C. 2007 Scalings and decay of fractal-generated turbulence. *Phys. Fluids* **19** (035103).

Laizet, S. & Lamballais, E. 2009 High-order compact schemes for incompressible flows: a simple and efficient method with the quasi-spectral accuracy. *J. Comp. Phys.* **228(16)**, 5989–6015.

Laizet, S. & Li, N. 2011 Incompact3d, a powerful tool to tackle turbulence problems with up to $o(10^5)$ computational cores. *Int. J. Numer. Methods Fluids* **67(11)**, 1735–1757.

Laizet, S. & Vassilicos, J. C. 2009 Multiscale generation of turbulence. *J. of Multiscale Modelling* **1**, 177–196.

Laizet, S. & Vassilicos, J. C. 2012 The fractal space-scale unfolding mechanism for energy-efficient turbulent mixing. *"Phys. Rev. E"* **86(4)**, 046302.

Mazellier, N. & Vassilicos, J. C. 2010 Turbulence without Richardson-Kolmogorov cascade. *Phys. Fluids* **22** (075101).

Mydlarski, L. & Warhaft, Z. 1998 Passive scalar statistics in high-peclet-number grid turbulence. *J. Fluid Mech.* **358**, 135–176.

Nagata, K., Suzuki, H., Sakai, H., Hayase, Y. & Kubo, T. 2008 Direct numerical simulation of turbulent mixing in grid-generated turbulence. *Inter. Review of PHYSICS* **132**, 014054.

Nicolleau, F., Salim, S. & Nowakowski, A.F. 2011 Experimental study of a turbulent pipe flow through a fractal plate. *J. Turbulence* **12**, 637046.

Parnaudeau, P., Carlier, J., Heitz, D. & Lamballais, E. 2008 Experimental and numerical studies of the flow over a circular cylinder at Reynolds number 3 900. *Phys. Fluids* **20**, 085101.

Shraiman, B.I. & Siggia, E.D. 2000 Scalar turbulence. *Nature* **6787**, 639–646.

Sirivat, A. & Warhaft, Z. 1983 The effect of a passive cross-stream temperature gradient on the evolution of temperature variance and heat flux in grid turbulence. *J. Fluid Mech.* **128**, 323–346.

Suzuki, H., Nagata, K., Sakai, H. & Ukai, R. 2010 High-schmidt-number scalar transfer in regular and fractal grid turbulence. *Phys. Scr.* **T142**, 014069.

Valente, P. & Vassilicos, J. C. 2011 The decay of turbulence generated by a class of multi-scale grids. *J. Fluid Mech.* **687**, 300–340.

Warhaft, Z. 2000 Passive scalars in turbulent flows. *Ann. Rev. Fluid Mech.* **32**, 203–240.

Wiskind, H.K. 1962 A uniform gradient turbulent transport experiment. *J. Geophysical Research* **67**, 30–33.